Ionics (2015) 21:365–371
DOI 10.1007/s11581-014-1188-y

ORIGINAL PAPER

Synthesis and electrochemical investigation of radial ZnO microparticles as anode materials for lithium-ion batteries

Guanghui Yuan · Gang Wang · Hui Wang · Jintao Bai

Received: 28 March 2014 / Revised: 21 May 2014 / Accepted: 15 June 2014 / Published online: 19 July 2014

Abstract ZnO microparticles with radial morphology are synthesized by hydrothermal method using polystyrene spheres as templates. The obtained ZnO microparticles have a size of 5–10 μm, which are assembled by lots of ZnO nanoparticles of ~10 nm. According to the starting materials used and characterization results observed, the formation process for the growth of the radial-like architecture is proposed. Electrochemical measurements indicate the good cycling performance and rate capability of the material for reversible lithium storage. The good electrochemical performance can be ascribed to the unique structure of the material, which can not only shorten the diffusion length for electrons and lithium ions but also provide a large specific surface area for lithium storage.

Keywords Zinc oxide · Radial morphology · Anode · Lithium-ion battery

Introduction

Lithium-ion battery is the most widely used rechargeable battery because of its high energy density and excellent service life [1–3]. Nowadays, increasing demand for high energy density batteries requires the development of alternative materials with high capacities. ZnO is regarded as one of the outstanding anode materials for next generation lithium-ion batteries. The electrochemical process of ZnO towards Li is more complicated than other transition-metal oxides, according to the previous studies [4, 5]. The discharge and charge process involves the decomposition/formation of ZnO and the formation/decomposition of Li–Zn alloy, which can be written as follows.

$$\mathrm{ZnO} + 2\mathrm{Li} \rightleftharpoons \mathrm{Zn} + \mathrm{Li_2O}$$
$$\mathrm{Zn} + \mathrm{Li} \rightleftharpoons \mathrm{LiZn}$$
$$\text{Total reaction}: \ \mathrm{ZnO} + 3\mathrm{Li} \rightleftharpoons \mathrm{LiZn} + \mathrm{Li_2O}$$

The theoretical specific capacity of ZnO electrode can be calculated by the following formula:

$$C_t\left(\mathrm{mA\,h\,g^{-1}}\right) = \frac{z \times F\left(\mathrm{C\,mol^{-1}}\right)}{M_w\left(\mathrm{g\,mol^{-1}}\right)} = \frac{z \times 96485(\mathrm{A{\cdot}s})}{M_w(\mathrm{g})} = \frac{z \times 26801(\mathrm{mA\,h})}{M_w(\mathrm{g})} = \frac{3 \times 26801(\mathrm{mA\,h})}{81.39(\mathrm{g})} = 987.87\left(\mathrm{mA\,h\,g^{-1}}\right)$$

In the formula, C_t, z, F and M_w denote the theoretical specific capacity, the transferred electron number in each structural unit, the Faraday constant and the molecular weight of the electrode material, respectively.

G. Yuan · G. Wang · J. Bai (✉)
National Key Laboratory of Photoelectric Technology and Functional Materials (Culture Base), National Photoelectric Technology and Functional Materials and Application International Cooperation Base, Institute of Photonics and Photon Technology, Northwest University, Xi'an 710069, China
e-mail: jintaobai@sina.cn

J. Bai
e-mail: baijt@nwu.edu.cn

G. Yuan
Department of Chemistry and Chemical Engineering, Ankang University, Shaanxi Ankang 725000, China

H. Wang
Key Laboratory of Synthetic and Natural Functional Molecule Chemistry (Ministry of Education), College of Chemistry & Materials Science, Northwest University, Xi'an 710069, China

Besides the attractive high theoretical capacity, other advantages such as low cost, easy to prepare and chemically stable make ZnO be extensively studied. Despite these considerable advantages, there are still some challenges for the application of ZnO in lithium-ion batteries: it always exhibits poor cycle ability even at low current densities and its capacity often drops quickly to <200 mA h g^{-1} after a few cycles. This is because that the electrode made from ZnO often suffers the loss of electrical contact arising from the severe volume expansion and contraction during repeated discharge–charge process, and the pulverization or the agglomeration of individual particles, which drastically reduces the total entrance/exit sites available for lithium ions [6–8].

Generally, morphology and structure are important factors affecting the electrochemical property of transition metal oxides. Microparticles with three-dimensional (3D) structure assembled by nanoparticles have been proved to be effective in improving the electrochemical performance of metal oxides [9–11]. This is because (1) the nanoparticles existed in the structure could shorten the diffusion length for electrons and lithium ions, and (2) the radial architectures with large surface/volume ratio could provide more active sites for lithium storage [12]. Thus, the design and synthesis of new electrode materials with 3D structural architectures will provide a tremendous opportunity to improve the lithium storage property. The synthesis of ZnO with 3D structures has been achieved by many different techniques including sputtering [13], electrochemical [14], chemical vapor depositions [15], template assisted sol–gel [16] and hydrothermal [15, 17] methods. During these methods, an appropriate alternative synthesis method based on a template, versatile in terms of size, extensive related to its applicability, but facile to be obtained and removed and, last but not least environmentally friendly represents a research priority of the topic. Hard cores such as carbonaceous spheres [18] or polystyrene spheres (PS) are commonly used as templates for a variety of metal oxides to achieve hollow structure particles [19–21], because the template cores are easily removed by either dissolution or calcination at high temperature.

In this work, we have designed a kind of nanoparticle assembled microscale ZnO 3D radial–like architecture through a facile hydrothermal route using PS spheres as templates. The possible formation process for the unique structure was proposed based on the starting materials used and the characterization results observed. The electrochemical performance of the obtained ZnO product as an anode material for lithium-ion batteries was investigated. It is found that the sample could exhibit good cycling performance and rate capability.

Experimental

Synthesis of mono-dispersed polystyrene

In a typical synthesis, 0.800 g polyvinylpyrrolidone stabilizer was dissolved in 30 ml ethanol in a three-necked round bottom flask fitted with a condenser and a magnetic stirrer. The reaction vessel was then heated to 70 °C under a nitrogen blanket and purged with nitrogen for 12 h at 70 °C. Then, a solution of Azoisobutyronitrile (0.120 g) pre-dissolved in styrene monomer (12.000 g) was added in with vigorous stirring. The styrene polymerization was allowed to proceed for 12 h and then cooled to ambient temperature. The white final powder was obtained via repeated centrifugation and washed with ethanol, and then vacuum dried overnight at 50 °C.

Synthesis of ZnO microparticles with radial morphology

To prepare the expected ZnO particles, 0.025 g PS and 0.140 g $ZnNO_3 \cdot 6H_2O$ were dropped separately into 15 ml ethanol. Then, 0.300 g $CO(NH_2)_2$ was dropped into another 15 ml solution mixed by 10 ml ethanol and 5 ml distilled water. After enduring ultrasonic radiation for 1 h, the two solutions were mixed together to form a homogeneous gel under vigorous stirring. Subsequently, this obtained white gel was transferred into a 50-ml Teflon autoclave. The autoclave was sealed and maintained at 80 °C for 12 h and then cooled down to ambient temperature naturally. The powder was separated from the solution by centrifugation, washed repetitively with distilled water and ethanol, and then dried at 80 °C over night. Finally, the powder was heated to 500 °C with 2 °C/min and kept for 1 h in air to obtain the expected ZnO.

Material characterization

Powder X-ray diffraction (XRD) patterns of samples were recorded by a Bruker D8 ADVANCE X-ray powder diffractometer using Cu Kα radiation (λ=0.15418 nm) at a scanning rate of 0.02° s^{-1} in the 2θ range 10–70°. Scanning electron microscopy (SEM) images of samples were measured by an FEI Quanta 400 ESEM-FEG (environmental scanning electron microscope-field emission gun) instrument with an accelerating voltage of 20 kV. Transmission electron microscopy (TEM) and selected area electron diffraction (SEAD) results of the samples were obtained on an FEI Tecnai G2 F20 S-TWIN instrument.

Electrochemical measurements

The composite anode was prepared by mixing 80 wt.% as-prepared ZnO, 10 wt.% polyvinylidene fluoride and 10 wt.% acetylene black in 1-methyl-2-pyrrolidinone. The resultant

slurry was painted onto a circular piece of nickel foam with 12 mm in diameter. After drying in a vacuum oven for 12 h at 80 °C, the nickel foam was pressed at 20 MPa in order to achieve good contact between the active material and nickel foam. The active material loading in each electrode was about 2 mg cm^{-2}. Lithium foils were used as the counter and the reference electrodes. The electrolyte was 1 M $LiPF_6$ dissolved in a mixture of dimethyl carbonate/diethyl carbonate/ethylene carbonate (1:1:1 by volume), and the separator was microporous polypropylene film. Coin-type (CR2025) test cells were assembled in a glove box filled with argon. The charge–discharge tests were carried out on a LAND battery program-control test system in a cut-off potential window of 0.005–3.0 V. Cyclic voltammetry (CV) was carried out on a CHI 660D electrochemical workstation at a scan rate of 0.1 mV s^{-1} in the potential range of 0–3.0 V versus Li/Li^+. Electrochemical impedance spectroscopy (EIS) was measured by using the same electrochemical workstation with the frequency range of 0.01–100 kHz.

Results and discussion

The crystal structure of the obtained product is firstly investigated by XRD (Fig. 1). As shown in the figure, the material possesses eight obvious diffraction peaks. Peaks at 2θ=31.8°, 34.4°, 36.3°, 47.5°, 56.6°, 62.9°, 66.4° and 68.0° are attributed to the reflections of (100), (002), (101), (102), (110), (103), (200) and (112) facets of the wurtzite hexagonal structured ZnO (space group P63mc, JCPDS No. 36-1451), respectively. No other detectable peaks from impurities are observed, indicating the high purity of the synthesized product. The strong and sharp peaks indicate that the as-obtained product is highly crystallized.

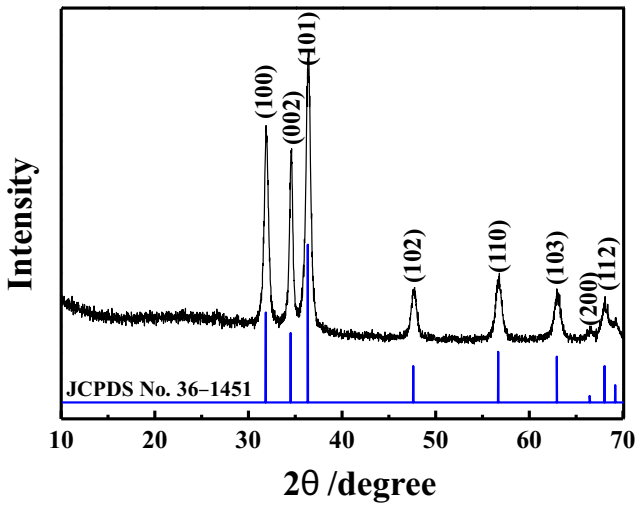

Fig. 1 XRD patterns of the synthesized ZnO sample

The morphology of the synthesized PS and the ZnO sample are measured by SEM (Fig. 2). Figure 2a shows a typical SEM image of the PS, from which one can see that the obtained particles have a uniform diameter of ~1.5 μm. Figure 2b and c gives the gradually enlarged SEM image of the ZnO sample. It can be observed from these figures that the sample mainly consists of a large number of radial microspheres of about 8 μm in diameter. To gain further insight into the morphology, the sample is studied by means of TEM measurement (Fig. 3). As can be seen in Fig. 3a, the several-branched radial microsphere has a hollow structure. The size of the hollow is about 1.5 μm, which is as big as the used PS. Such a result indicates

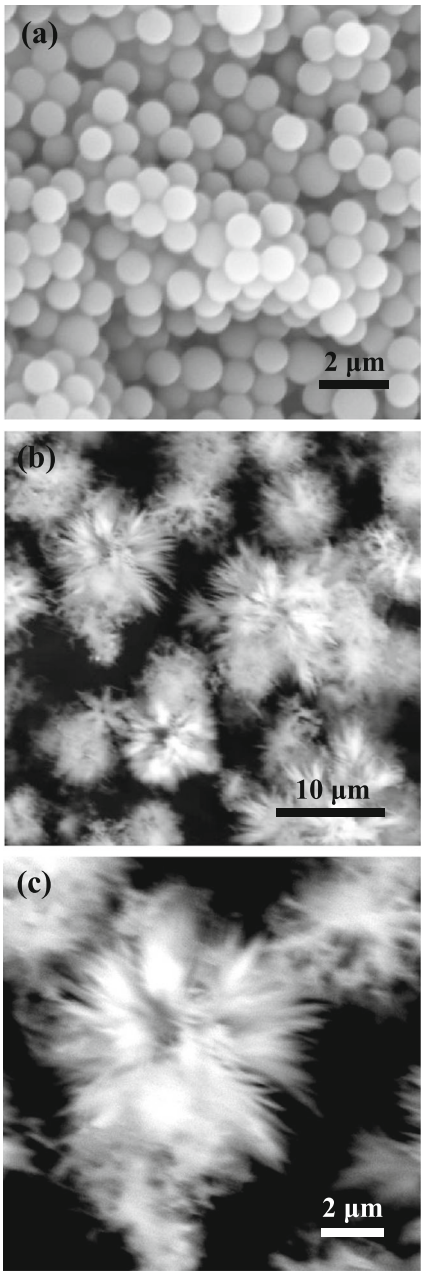

Fig. 2 SEM images of **a** PS, and **b**, **c** radial ZnO microparticles

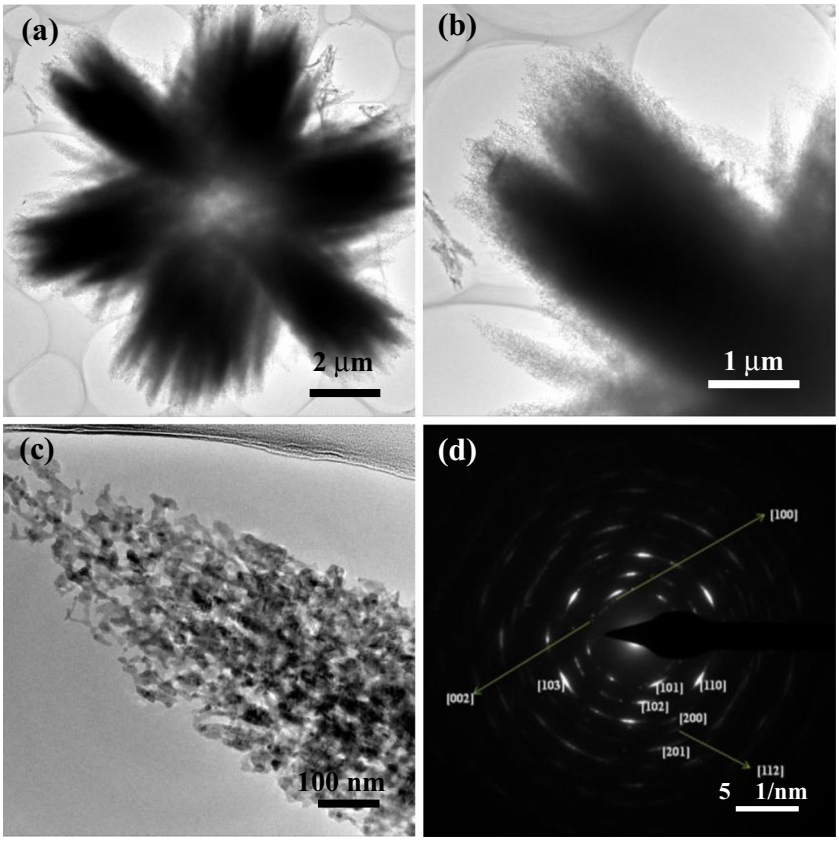

Fig. 3 **a**–**c** Gradually enlarged TEM images of a radial ZnO microparticle, and **d** SAED pattern of the ZnO sample

the hollow structure was formed by the loss of the PS. Careful observation on the surface of a ZnO tip indicates that each branch has a mesoporous structure, composed of numerous nanoparticles with a size of several nanometers (Fig. 3b and c). The SAED pattern of the ZnO (Fig. 3d) is composed of continuous rings and can be indexed with the hexagonal ZnO phase, which demonstrates that the sample is polycrystalline.

Figure 4 depicts the possible formation process of the radial ZnO microparticles according to the template used and the micrography results obtained. In the experiment environment, homogeneous nucleation of ZnO arose on the surface of the PS and then crystallized momentarily to form nanoparticles with high-surface energy at the initial stage. Under super-critical conditions in autoclave, the original ZnO nanoparticles on the surface of the PS became the crystallization centre. It is well known that the Ostwald ripening process usually occurs in the presence of water [22, 23]. Therefore, with the existence of a little water in the reaction system, a slow Ostwald ripening occurred successfully. Furthermore, different solvents have different boiling points in super-critical conditions [24, 25]. Thus ethanol in the mixed solution might release lots of gas bubbles during the Ostwald ripening process, which made ZnO crystals slowly grew or aggregated along the crystallization centre on the surface of the PS to form several-branched solid microparticles to minimize the interfacial energy. When calcined in air, PS in the sample was oxidized to generate H_2O and CO_2, while ZnO microparticles thus would be obtained due to

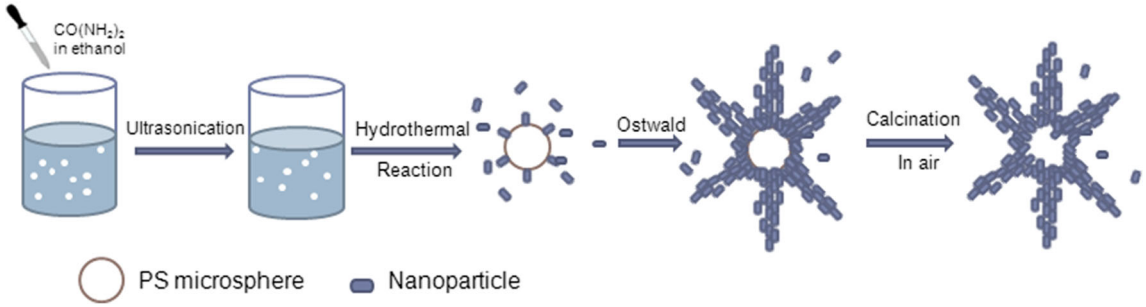

Fig. 4 Schematic for the formation process of the hollow radial ZnO particles

their structural rigidity and their hollow radial morphology could be maintained.

The electrochemical property of the ZnO microparticles as anode materials for lithium-ion batteries are examined by CV. The CV curves of the electrode in the first three cycles are recorded at a scan rate of 0.1 mV s^{-1} between 0 and 3.0 V (Fig. 5a). In the first cathodic scan, only one strong peak at ~0.2 V appears, which can be ascribed to the reduction of ZnO into Zn, the formation of Li–Zn alloy, and the formation of the solid electrolyte interphase (SEI) layer. During the subsequent anodic scan, several different oxidation peaks locate at 0.3, 0.5, and 0.7 and 1.4 V can be observed. The first three peaks indicate the occurrence of a multi-step dealloying process of Li–Zn alloy and the decomposition of the organic-like layer, while the peak at 1.4 V is concerned with the decomposition of Li_2O. After the first cycle, the CV curves exhibit good reproducibility and almost coincide in shape, indicating high reversibility of the electrode.

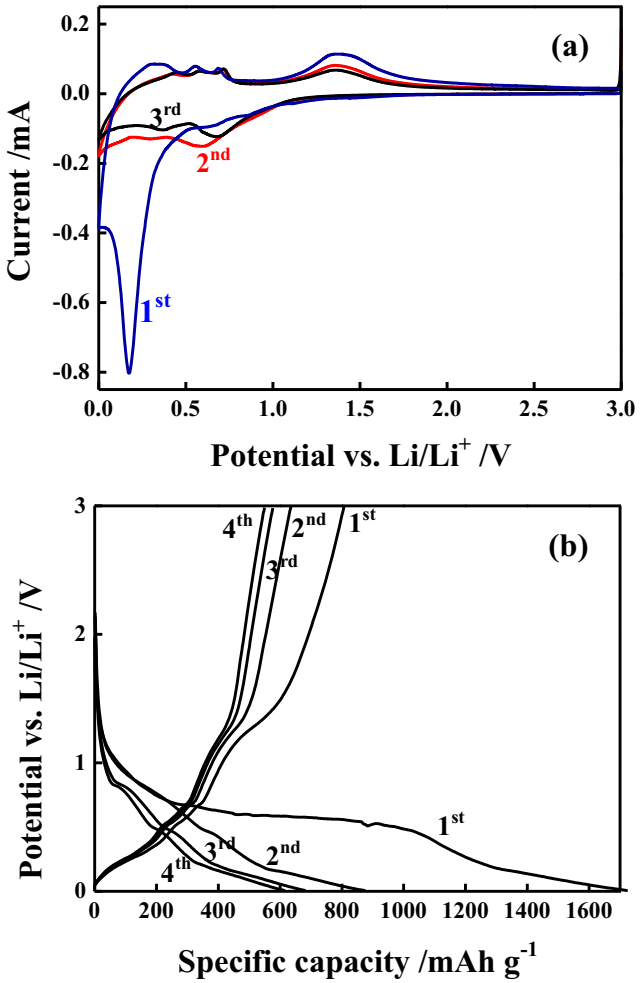

Fig. 5 **a** CV curve of the synthesized ZnO electrode; **b** charge–discharge profiles of the synthesized ZnO electrode at the current density of 50 mA g^{-1}

Figure 5b illustrates the galvanostatic discharge–charge curves of the ZnO electrode at the first, second and third cycles with a current density of 0.1 A g^{-1}. As can be seen in the figure, the plateaus on the voltage profiles are in agreement with the CV peaks shown in Fig. 5a. The electrode delivers an initial discharge capacity of 1,725 mA h g^{-1}, which is much higher than its theoretical value of 987 mA h g^{-1}. Such a result suggests extra lithium storage during the SEI layer formation. The initial charge capacity is 807 mA h g^{-1}, resulting in an initial coulombic efficiency of ~47 %. After the first cycle, the discharge and charge curves tend to overlap, suggesting a relatively steady state of the lithiation/delithiation process.

The cycling performance of the electrode over 100 cycles of discharge and charge at a constant current density of 0.2 A g^{-1} and the corresponding coulombic efficiency are shown in Fig. 6a. It can be seen from it that the discharge and charge capacities decreased gradually at the initial 10 cycles. However, from the 11th cycle onward, the ZnO electrode shows the fascinating cycling stability. The coulombic efficiency steadily reaches around 99 % accompanied by the cycle number increasing. After 100 cycles, a reversible capacity of 320 mA h g^{-1} is still retained, corresponding to about 75 % of the reversible capacity in the 11th cycle. The rate capability of the ZnO electrode from 0.1 to 1.6 A g^{-1} is also tested and displayed in Fig. 6b. As expected, the electrode capacity

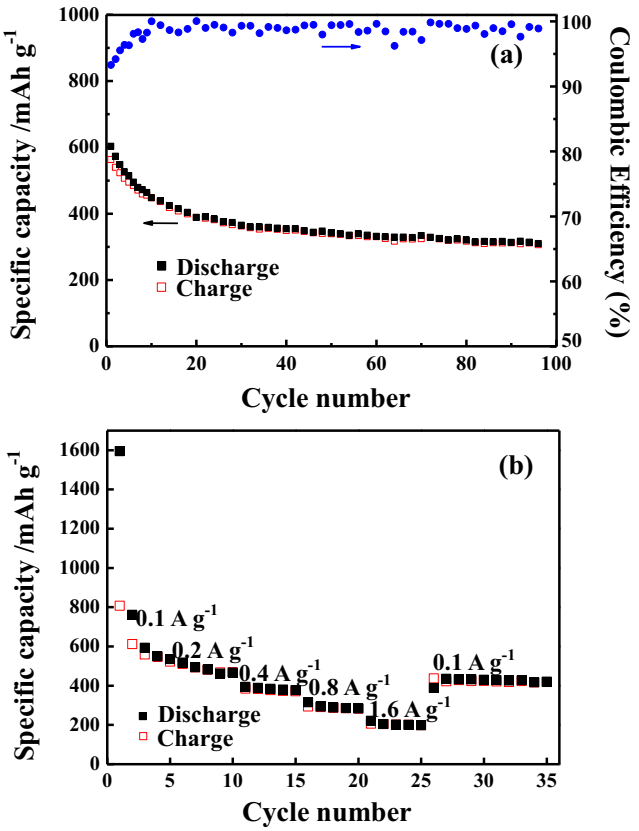

Fig. 6 **a** Cycle performance and **b** rate performance of the hollow radial ZnO electrode

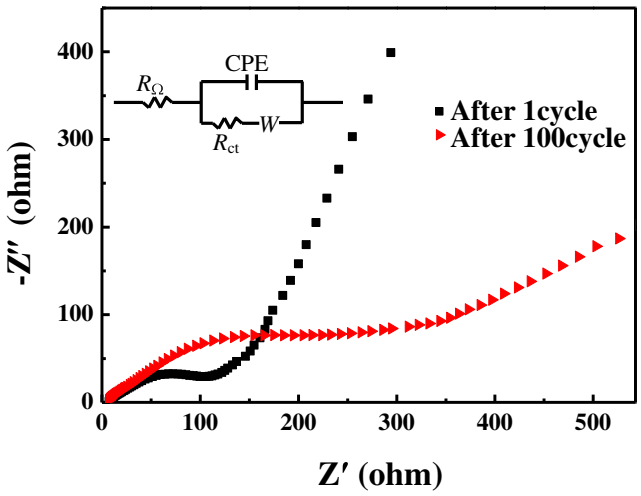

Fig. 7 Nyquist plots of the ZnO anode with the whole frequency region of 100 kHz to 0.01 Hz

reduces upon increasing the charge and discharge rates. At a low current density of 0.1 A g^{-1}, the hollow radial ZnO exhibits high reversible capacities of 807 mA h g^{-1}. At the higher current densities of 0.2, 0.4, and 0.8 A g^{-1}, the discharge capacities of each period are 518, 393, and 315 mA h g^{-1}, and the charge capacities are 510, 385, and 295 mA h g^{-1}, respectively. Even at 1.6 A g^{-1}, the electrode still achieves a high reversible capacity of 206 mA h g^{-1}. When the current density returns back to the initial 0.1 A g^{-1}, the electrode delivers a stable reversible capacity of nearly 500 mA h g^{-1}, confirming a good reversibility and rate capability of the radial ZnO anode.

EIS measurements are carried out in order to analysis the conductivity of the ZnO electrode. In the equivalent circuit (inset in Fig. 7), R_Ω and R_{ct} are the ohmic resistance (total resistance of the electrolyte, separator, and electrical contacts) and charge transfer resistance, respectively. CPE is the constant phase-angle element, involving double layer capacitance, and *W* represents the Warburg impedance reflecting the solid-state diffusion of lithium ion into the bulk of the active materials [26–28]. The Nyquist plots for the ZnO electrode of 1st cycle and 100th cycle are similar, displaying a typical characteristic shape with a semicircle in the high-frequency range, which could be assigned to the R_{ct}, and an inclined line in the low frequency range, which represents the *W*. In general, the smaller the diameter of a semicircle is, the lower the charge transfer resistance of an electrode. The high-to-medium frequency semicircle after the first cycle is only about 120 Ω. Considering the formation of SEI is completed, the small impedance can be mainly attributed to the radial structure, which enlarges the electrolyte/ZnO contact area, shortens the Li ion diffusion length in ZnO nanoparticles. After 100 cycles, the high-to-medium frequency semicircle becomes about double size. The total impedance growth could be attributed to possible landslide of the hollow radial structure after many cycles and the agglomeration of the ZnO particles and loss of its contact with the conductor in anode.

Table 1 Literature comparison between the electrochemical performances of ZnO-based anodes for Li-ion batteries

Sample (morphology)	Reversible capacity (mA h g^{-1})	Cycle number	Potential (V vs. Li^+/Li)	Current density	Ref.
ZnO (radial hollow microparticles)	320	100th	0.005–3.0	0.2 A g^{-1}	This work
ZnO (nanowire)	252	30th	0.005–3.0	0.12 A g^{-1}	[7]
ZnO (flower-like microaggregates)	179	200th	0.02–2.8	1C	[10]
ZnO (dandelion-like nanorod arrays)	~ 310	40th	0–3.0	0.25 A g^{-1}	[11]
ZnO-U/PC	654	100th	0.1–3.0	0.1 A g^{-1}	[28]
ZnO-C (flower-like nanowall arrays)	316	50th	0–3.0	0.5C	[29]
ZnO (flower-like arrays)	238	50th	0–3.0	0.5C	[29]
ZnO (microrod)	150	50th	0–3.0	0.5 A g^{-1}	[30]
ZnO (microrod arrays grown on Copper)	500	100th	0–3.0	0.5 A g^{-1}	[30]
ZnO (nanorod)	358	30th	0.3–3.0	0.05 A g^{-1}	[31]
TiO_2-coated ZnO	447	30th	0.3–3.0	0.05 A g^{-1}	[31]
ZnO (hexagonal nanoplates)	~500	50th	0–3.0	0.5C	[32]
ZnO (nanowall arrays)	~200	40th	0.02–2.0	0.12 A g^{-1}	[33]
ZnO/SnO_2 (micro-crystals)	~400	40th	0.02–2.0	0.12 A g^{-1}	[33]
ZnO (nanosheets grown on copper)	~400	100th	0.01–3.0	0.5 A g^{-1}	[34]
ZnO (flower-like microparticles)	~200	50th	0.02–3.0	0.12 A g^{-1}	[35]
ZnO-Au (flower-like nanostructures)	392	50th	0.02–3.0	0.12 A g^{-1}	[35]
ZnO-C (flower-like nanospheres)	~400	30th	0.05–2.5	0.5C	[36]
ZnO@GN (framework)	~460	50th	0.01–3.0	1C	[37]

Based on the above electrochemical investigations on the ZnO electrode, it is worth noting that our prepared radial material exhibited superior electrochemical performance in comparison with those presently reported results, as shown in Table 1. It is to be noted here that the electrochemical characteristics upon reversible reaction with lithium are even more remarkable when considering that our proposed sample is pure ZnO, without any carbon-coated agents or graphene additives. However, in comparison with its theoretical capacity, the electrode is not excellent enough in lithium storage capacity. The recent work proved that the incorporation of carbon materials with metal oxides, such as carbon-coated, carbon nanotube-doped, or graphene nanosheet-loaded metal oxides, can improve the lithium storage property of metal oxides [35–40]. Therefore, the combination of carbon materials with the sample may further enhance its electrochemical performance.

Conclusion

ZnO microparticles with radial morphology were synthesized successfully through a facile hydrothermal route using PS spheres as templates. The synthesized ZnO of 5–10 μm was composed and assembled by numerous nanoparticles in a diameter of ~10 nm. When tested as an anode material for lithium-ion batteries, the material exhibited a high initial discharge and charge capacity of 1,725 and 807 mA h g^{-1}, respectively. Cycling performance indicated that the electrode kept a reversible capacity of about 320 mA h g^{-1} after 100 cycles at 0.2 A g^{-1}. The good electrochemical performance was attributed to the unique radial structure, which could provide plenty of active sites and enlarge the electrolyte/ZnO contact area for lithium storage.

Acknowledgments This work was supported by the financial supports of the National Natural Science Foundation of China (Nos. 21301140 and 21061130551), and the Natural Science Foundation of Shaanxi Province (Nos. 2013JQ2004 and 2013JM2009).

References

1. Liu J (2013) Adv Funct Mater 23:924
2. Chandrashekar S, Trease NM, Chang HJ, Du LS, Grey CP, Jerschow A (2012) Nat Mater 11:311
3. Zhang YG, Zhao Y, Konarov A, Gosselink D, Soboleski HG, Chen P (2013) J Power Sources 241:517
4. Belliard F, Connor PA, Irvine JTS (1999) Ionics 5:5450
5. Yang GZ, Song HW, Cui H, Liu YC, Wang CX (2013) Nano Energy 2:579
6. Kushima A, Liu XH, Zhu G, Wang ZL, Huang JY, Li J (2011) Nano Lett 11:4535
7. Wang JZ, Zhang N, Yu JX, Yang DR (2011) Mater Res Bull 46:2378
8. Zhou YN, Li WJ, Fu ZW (2012) Electrochim Acta 59:435
9. Keon TP, Xia F, Sung WK, Kim SB, Song T, Paik U, Park W (2013) J Phys Chem C 117:1037
10. Cauda V, Pugliese D, Garino N, Sacco A, Bianco S, Bella F, Lamberti A, Gerbaldi C (2014) Energy 65:639
11. Wang H, Pan Q, Cheng Y, Zhao J, Yin G (2009) Electrochim Acta 54: 2851
12. Rolison DR, Long JW, Lytle JC, Fischer AE, Rhodes CP, McEvoy TM, Bourga ME, Lubersa AM (2009) Chem Soc Rev 38:226
13. Gazia R, Chiodoni A, Bianco S, Lamberti A, Quaglio M, Sacco A, Tresso E, Mandracci P, Pirri CF (2012) Thin Solid Films 524:107
14. Elias J, Tena-Zaera R, Lévy-Clément C (2008) J Electroanal Chem 621:171
15. Podrezova LV, Porro S, Cauda V, Fontana M, Cicero G (2013) Appl Phys A 113:623
16. Bechelany M, Amin A, Brioude A, Cornu D, Miele P (2012) J Nanopart Res 980:1
17. Rivera VF, Auras F, Motto P, Stassi S, Canavese G, Celasco E, Bein T, Onida B, Cauda V (2012) Chem Eur J 19:14665
18. Patrinoiu G, Calderón-Moreno JM, Culita DC, Birjega R, Ene R, Carp O (2013) J Solid State Chem 202:291
19. Zhang J, Tu JP, Cai GF, Du GH, Wang XL, Liu PC (2013) Electrochim Acta 99:1
20. Wang X, Liu J, Feng X, Guo M, Sun D (2008) Mater Chem Phys 112:319
21. Eliasa J, Utkea I, Yoon S, Bechelany M, Weidenkaff A, Michlera J, Philippe L (2013) Electrochim Acta 110:387
22. Zhang X, Qiao R, Kim JC, Kang YS (2012) Cryst Growth Des 8: 2609
23. Rao J, Yu A, Shao C, Zhou X (2012) ACS Appl Mater Interfaces 4: 5346
24. Suriyarak S, Weiss J (2014) Colloids Surf A Physicochem Eng Asp 446:71
25. Hoang TKN, Deriemaeker L, La VB, Finsy R (2004) Langmuir 20: 8966
26. Han F, Li D, Li WC, Lei C, Sun Q, Lu AH (2012) Adv Funct Mater 1:1
27. Zhou G, Wang DW, Yin LC, Li N, Li F, Cheng HM (2012) ACS Nano 6:3214
28. Shen XY, Mu DB, Chen S, Wu BR, Wu F (2013) ACS Appl Mater Inter 8:3118
29. Wu Z, Qin LM, Pan QM (2011) J All Comp 509:9207
30. Huang XH, Wu JB, Lin Y, Guo RQ (2012) Int J Electrochem Sci 7: 6611
31. Lee JH, Hon MH, Chung YW (2011) Appl Phys A Mater Sci Process 102:545
32. Abbas SM, Hussain ST, Ali S, Ahmad N, Ali N, Abbas S (2013) J Mater Sci 48:5429
33. Ahmad M, Ying S, Sun H, Shen W, Zhu J (2012) J Solid State Chem 196:326
34. Huang XH, Xia XH, Yuan YF, Zhou F (2011) Electrochim Acta 56: 4960
35. Ahmad M, Shi Y, Nisar A, Sun H, Shen W, Wei M, Zhu J (2011) J Mater Chem 21:7723
36. Li F, Yang L, Xu G, Huang X, Yang X, Wei X, Ren Z, Shen G, Han G (2013) J All Comp 577:663
37. Hsieh C, Lin C, Chen Y, Lin J (2013) Electrochim Acta 30:359
38. Yang SJ, Nam S, Kim T, Im JH, Jung H, Kang JH, Wi S, Park B, Park CR (2013) J Am Chem Soc 20:7394
39. Yu MP, Shao DL, Lu FY, Sun X, Sun HT, Hu T, Wang GK, Sawyer S, Qiu H, Lian J (2013) Electrochem Commun 34:312
40. Mehmet OG, Cetinkaya T, Tocoglu U, Akbulut H (2014) Microelectron Eng 118:54